Submitted to the Annals of Applied Statistics
2017 Vol. , No. , 1–8
arXiv: arXiv:0000.0000

SUPPLEMENT A: PRELIMINARY STATISTICAL ANALYSIS OF THE IN VITRO THREE-CUBE FRET DATA SET

By Jan-Otto Hooghoudt, Margarida Barroso and Rasmus Waagepetersen

In this supplementary material to "Towards Bayesian Inference of the Spatial Distribution of Proteins from Three-Cube FRET Data" we present a preliminary statistical analysis of the in vitro transferrin attached to polylysine slides three cube FRET data set. We start by describing the experimental set-up and sample preparation in Section 1 and discuss the channel data set extracted from these samples in Section 2. Then we study the influence that photobleaching of the donors and acceptors has on the intensity signal for the remeasurements in the three channels in Section 3, and we present simple non-Bayesian methods for estimating the K and G factors in Section 4 and 5, respectively. Methods for estimating the G_A and G_D factors are presented in Section 6 and an estimate of the ratio of the quantum efficiencies in the detector D- and A-channel is given in Section 7. We conclude by obtaining an estimate of M_D in Section 8.

1. The experimental set-up. Fourteen glass cover slips coated with polylysine have been prepared to contain various abundances of donor and acceptor fluorophores attached to it. Briefly, the procedure is as follows. Transferrin is labeled solely with donor fluorophores or solely with acceptor fluorophores, leading to Tfn-D and Tfn-A molecules. As donor the Alexa-488 fluorophore ($q_D = 0.92$) is used and as acceptor the Alexa-555 fluorophore ($q_A = 0.10$) is used. The Förster distance of the Alexa-488 and Alexa-555 fluorophore pair is 7 nm (Johnson, 2010). Solutions containing concentrations of approximately 2, 4 or 8 μg/ml of solely Tfn-D or solely Tfn-A are prepared, and glass cover slips coated with polylysine are incubated for a certain period with Tfn-D and/or Tfn-A solution. The procedure followed to bind transferrin to polylysine plates is described in more detail in Wallrabe et al. (2006).

In Table 1 the sample preparation set-up is shown. The samples 1-3 contain only donor fluorophores, while samples 4-6 consist of only acceptor fluorophores. The samples 7-14 consist of mixtures of donor and acceptor fluorophores. We note that the samples denoted as sample 1, 2 and 3 in the main article correspond to, respectively, the samples 7, 9 and 11 in Table 1.

	Sample number													
	1	2	3	4	5	6	7	8	9	10	11	12	13	14
$[A]_{sol}$	-	-	-	2	4	8	2	4	4	8	4	8	6	8
$[D]_{sol}$	2	4	8	-	-	-	4	8	4	8	2	4	2	2

TABLE 1

Sample preparation set-up for transferrin attached to polylysine slides. The solution concentrations of Tfn-A ($[A]_{sol}$) and Tfn-D ($[D]_{sol}$) applied are stated for each sample in units of $\mu g/ml$.

2. The channel data set. Each sample (see Table 1) has been measured at three sites. At each site three-cube FRET channel data is obtained on a square grid containing 512×512 square pixels. The pixel side length is 0.279 μm and the focal volume depth is approximately 5 pixels (1.4 μm) (Wallrabe et al., 2007).

In order to obtain sufficient photon count statistics—that is sufficiently high signal-to-noise ratio to apply our Bayesian inference method—each sample has been remeasured ten times.[1] We then create an aggregated dataset—the *aggregated channel dataset*—by summing pixel wise over the ten measured intensities for each channel. By remeasuring the sample instead of increasing the measurement time, we obtain information concerning: the amount of photobleaching occurring for remeasurements (see Section 3) and the pixel intensity variance in the three channels. The latter information gives the possibility to compare the empirical pixel intensity mean-variance relationship with the one implied by our statistical model, as well as to obtain estimates for G_D and G_A (see Section 6).

All three channels are corrected for background emission and the DA-channel is also corrected for spectral bleedthrough by the methods described in Elangovan et al. (2003). In the following, DA-channel data (Y_{DA}) refers to the intensities corrected for bleedthrough and background emission and the DD- and AA-channel data (Y_{DD} and Y_{AA}, respectively) to the intensities corrected for background emission. We will refer to a sample by its sample number (see Table 1).

In Figure 1 the channel intensity images of the aggregated channel dataset of sample 9 are shown in terms of gray levels. In plot a) and b) there are some very low intensity regions (black spots) and in the upper left corner of plot c) most of the DA-channel intensities are zero. These artefacts are due to improper sample preparation. Therefore the statistical analysis as

[1] For a typical three-cube FRET experiment less than 10 photons counts per pixel are registered by the detector in the DA-channel (Pawley, 2006, Chapter 2; Clegg, 1996, Chapter 1).

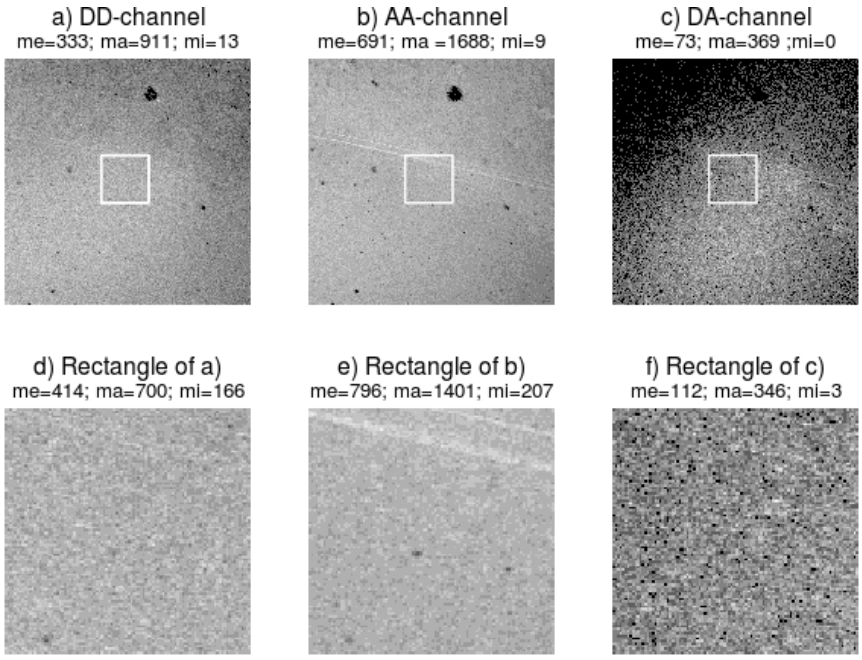

FIG 1. *Channel intensity images of the aggregated channel dataset of sample 9, site 2. a) DD-channel, b) AA-channel, c) DA-channel. Plots a)-c) consist each of 512×512 pixels: Figures d-f) show enlargements of the square subregions of the figures a-c), each consisting of 100×100 pixels. Above each plot is stated the mean (me), maximum (ma) and minimum (mi) pixel intensity value in the image. In each image the gray levels are constructed by using ten equally spaced intervals between zero and the maximum value of the image. Black/white refers to the lowest/highest intensity interval.*

presented in the following sections are based on the channel data of the central square section consisting of 100×100 pixels (the white squares in plots a)-c).

In the following we will occasionally for any site and sample make use of the following generic notation. We denote the pixel intensity of pixel i measured in channel $k = DD, DA, AA$ and for measurement number $m = 1, \ldots, 10$ by $Y_k^{i,m}$. The *sample mean intensity*—taken over the 100×100 pixels—for channel k and measurement number m is denoted by $\bar{Y}_k^{\cdot m}$, that is $\bar{Y}_k^{\cdot m} = \frac{1}{1e4} \sum_{i=1}^{1e4} Y_k^{i,m}$. The *pixel mean intensity* for pixel i for the 10 remeasurements m for channel k will be denoted by $\bar{Y}_k^{i\cdot}$, that is $\bar{Y}^{i\cdot} = \frac{1}{10} \sum_{m=1}^{10} Y_k^{i,m}$. The *sample grand mean intensity* taken over the 100×100 pixels and the 10 remeasurements will be denoted by $\bar{\bar{Y}}_k = \frac{1}{10} \sum_{m=1}^{10} \bar{Y}^{\cdot m}$.

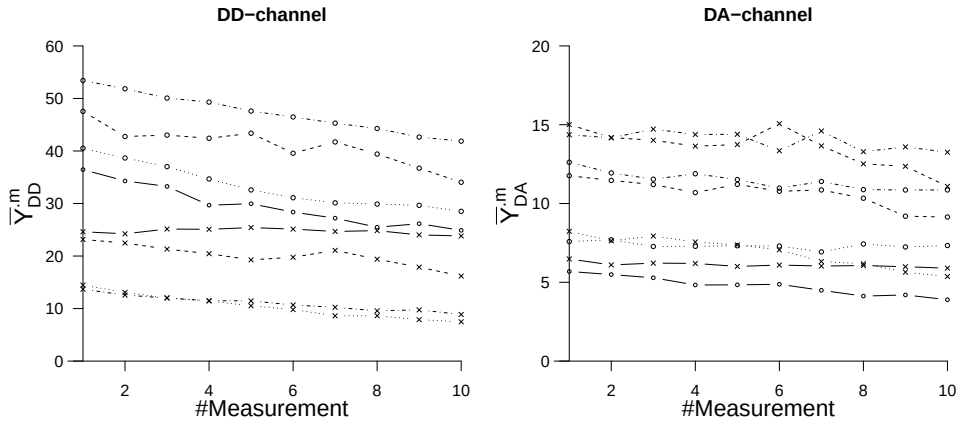

FIG 2. *Sample mean intensity versus measurement number shown for site 2 for the D+A samples: left) DD-channel, right) DA-channel. Solid-circle: sample 7 ; dashed-circle: sample 8; dotted-circle: sample 9; dashed-dotted-circle: sample 10; solid-triangle: sample 11; dashed-triangle: sample 12; dotted-triangle: sample 13; dashed-dotted-triangle: sample 14.*

3. Photobleaching due to remeasuring. In Figure 2 the sample mean intensity is shown as a function of the remeasurement number for the DD- and DA-channel, for site 2 of the D+A samples. Clearly, the sample mean pixel intensity has a slightly decreasing trend as a function of the measurement number. The decrease in intensity between measurement one and ten is roughly between 10–30% for all samples and for both channels. The same amount of decrease in intensity occurs for the AA-channel (not shown). The same analysis applied to the sites 1 and 3 of the D+A samples showed similar results as just discussed for site 2.

We note that the intensity remeasurements could be incorporated in our inference procedure by using the product of likelihoods for each measurement i.e. in equation (3.1) in the main article we could replace each of the likelihood terms $p(y_k|\psi, \mathbf{x}), k = DD, DA, AA$ by $\prod_{m=1}^{M} p(y_k^m|\psi, \mathbf{x})$ with $M = 10$ the total number of measurements and y_k^m the observed intensity for channel k and measurement m. Thereby, a possible way to account for the decreasing linear trend in the pixel intensities due to bleaching is the following. Define $\mu_k^{i,1}$—as in (2.2) and (2.3) in the main article—to be the channel mean pixel intensity for measurement number 1 for pixel i and channel $k = DD, DA, AA$, and relate the mean pixel intensity $\mu_k^{i,m}$ for the remeasurements $m = 2, \ldots, 10$ to $\mu_k^{i,1}$ by

$$\mu_k^{i,m} = \mu_k^{i,1} - a(m-1)$$

and include a as a parameter in the model. For simplicity, however, we have

chosen instead to create the aggregated photon count data set, to view it as resulting from one measurement and to apply our Bayesian inference procedure to this aggregated data set.

4. Estimate of the *K*-factor. The K-factor can be obtained experimentally by the preparation of a sample which contains equimolar concentrations of donor and acceptor fluorophores (Chen et al., 2006). Then by measuring the sample mean intensities in the three channels $(\bar{\bar{Y}}_{DD}, \bar{\bar{Y}}_{DA}, \bar{\bar{Y}}_{AA})$ an estimate for K is obtained by

$$K = \frac{\bar{\bar{Y}}_{DD} + \bar{\bar{Y}}_{DA}/G}{\bar{\bar{Y}}_{AA}}.$$

For a sample with unequimolar donor and acceptor concentrations [A] and [D] this relations becomes

$$K = \frac{[\mathrm{A}]}{[\mathrm{D}]} \frac{\bar{\bar{Y}}_{DD} + \bar{\bar{Y}}_{DA}/G}{\bar{\bar{Y}}_{AA}},$$

(Chen et al., 2006). The ratio $b_A = \bar{\bar{Y}}_{AA}/[\mathrm{A}]$ can be found as the slope of a regression line for pairs $([\mathrm{A}], \bar{\bar{Y}}_{AA})$ for samples with varying concentration $[A]$ and arbitrary donor concentration. Similarly, $b_D = (\bar{\bar{Y}}_{DD} + \bar{\bar{Y}}_{DA}/G)/[\mathrm{D}]$ can in principle be found as the slope of a regression line for pairs $([\mathrm{D}], \bar{\bar{Y}}_{DD} + \bar{\bar{Y}}_{DA}/G)$. This, however, would require knowledge of G. In our data set, on the other hand, we have access to donor only samples and we can thus replace $\bar{\bar{Y}}_{DD} + \bar{\bar{Y}}_{DA}/G$ for a sample with both donors and acceptors of concentrations [D] and [A] with $\bar{\bar{Y}}_{DD}$ for a sample only containing donors of concentration [D].

In Figure 3 a) $\bar{\bar{Y}}_{DD}$ is plotted against $[\mathrm{D}]_{\mathrm{sol}}$ for the donor only samples 1-3.[2] The resulting slope of the regression line (of intercept 0) is $b_D = 10.6$. Further, in Figure 3 b), $\bar{\bar{Y}}_{AA}$ is plotted versus the sample acceptor concentration $[\mathrm{A}]_{\mathrm{sol}}$ for acceptor only as well as D+A samples, and the slope b_A of the least squares line—found for a fixed intercept of zero—is 15.4. Thereby, we find as an estimate for the K-factor rounded to one decimal: $\widehat{K} = b_D/b_A \approx 0.7$.

5. Estimate of the *G*-factor. The sample mean unquenched donor intensities for the D+A samples (samples 7-14) should scale with the applied

[2]Because the true donor [D] and acceptor [A] concentrations in the samples are unknown, we use, respectively, the donor and acceptor concentrations $[\mathrm{D}]_{\mathrm{sol}}$ and $[\mathrm{A}]_{\mathrm{sol}}$ applied to prepare the samples, to find estimates for b_D and b_A.

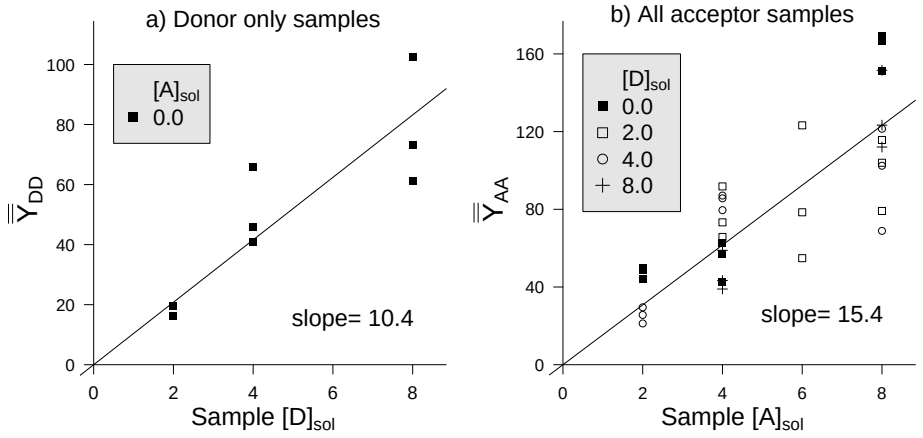

FIG 3. *Sample grand mean pixel intensity versus applied solution concentration. a) DD-intensity vs donor solution concentration for each of the three sites of the donor only samples (samples 1-3) , b) AA-intensity vs acceptor sample concentration for for each of the three sites of the acceptor only (samples 4-6) and the D+A samples (samples 7-14).*

sample donor solution concentration [D] by the same slope b_D as determined in the previous section. This observation provides a method to obtain a rough estimate for the G-factor.

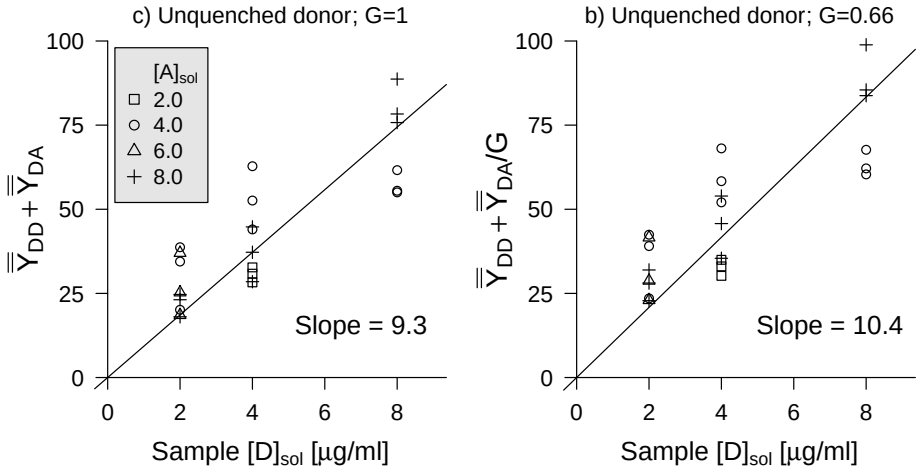

FIG 4. *Sample grand mean intensity of unquenched donor $\bar{\bar{Y}}_{DD} + \bar{\bar{Y}}_{DA}/G$ versus sample donor concentration for each of the three sites of the D+A samples (samples 7-14): a) $G = 1$, b) $G = 0.66$. In plot b) the value of G has been tuned in order to obtain a least square line with a slope of 10.4. The least square lines are fitted in both plots with a fixed intercept of zero.*

Figure 4 shows a similar plot as in Figure 3 a) where $\bar{\bar{Y}}_{DD}+\bar{\bar{Y}}_{DA}$ is plotted versus the applied donor solution concentration $[D]$ for the D+A samples. For this plot the slope of the least square estimate is 9.3, which is close to but slightly lower than the previous found estimate of $b_D = 10.4$. Since we have $\bar{\bar{Y}}_{DD} + \bar{\bar{Y}}_{DA}/G = b_D[D]$, this suggests a value of G less than one. We now simply tune G so that the regression for $\bar{\bar{Y}}_{DD} + \bar{\bar{Y}}_{DA}/G$ versus $[D]$ has the slope $b_D = 10.4$. This happens for $G = 0.66$, see Figure 4 b). We round this value to one decimal and find as an estimate for the G-factor, $\widehat{G} = 0.7$.

6. Assessment of mean-variance relation for polylysine data. As each sample has been remeasured ten times, for pixel i we have observations $Y_k^{i,m}$ where $m = 1, \ldots, 10$ is the index of the replicates. Apart from a slight decrease in intensity due to bleaching (see Section 3), we can view the $Y^{i,m}$ as independent and identically distributed. If we further ignore for the moment the additive noise, then the statistical model—equations (2.1)–(2.3) in the main article—predicts a log-log linear relationship between the pixel mean μ_k^i and the pixel variance $\sigma_k^{2,i}$ of $Y_k^{i,m}$. E.g. for the DD-channel,

$$\log \sigma_{DD}^{2,i} = \log G_D + \log \mu_{DD}^i,$$

with G_D the amplification factor of the detector in the D-channel. Now, for each pixel we compute empirical means $\bar{Y}_k^{i\cdot} = \sum_{m=1}^{M} Y_k^{i,m}$ and empirical variances

$$s_k^{2,i} = \frac{1}{M-1} \sum_{m=1}^{M} \left(Y_k^{i,m} - \bar{Y}_k^{i\cdot}\right)^2, \; k = DD, AA$$

with $M = 10$ the total number of measurements. Figure 5 shows for the two channels $k = DD, AA$ the empirical log variances $\log s_k^{2,i}$ against the log empirical means $\log \bar{Y}_k^{i\cdot}$. By fitting a regression line with a slope of 1 through the points, the intercept provides a rough estimate of respectively $\log G_D$ and $\log G_A$. The intercept is 2.0 for the DD-channel (plot a)) and 1.7 for the AA-channel (plot b)). Thereby we find, rounded to one decimal, the estimates $\widehat{G}_D = \exp(2.0) \approx 7.4$ and $\widehat{G}_A = \exp(1.7) \approx 5.5$.[3]

7. Estimate of the ratio of the detector quantum efficiencies. By the definition of the G-factor, as stated in the Appendix of the main article,

$$\frac{Q_D}{Q_A} = \frac{G_A q_A}{G G_D q_D}.$$

[3]We note that least square estimates for the slopes of the regression lines in Figure 5 are 1.1 ± 0.2 for the DD- as well as the AA-channel, which is indeed close to one as predicted by the statistical model.

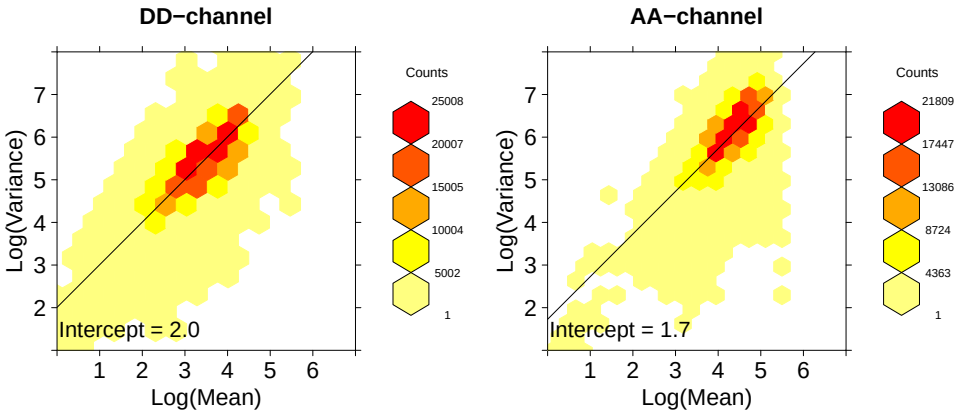

FIG 5. *Smoothed log-log scatterplot of the empirical pixel intensity variances* $s_k^{2,i}$ *versus the corresponding empirical pixel intensity means* $\bar{Y}_k^{i\cdot}$. *In both plots the least squares line is fitted for a fixed slope of one. For plot a) the DD-channel intensity data is used for each of the three sites of the donor only samples (samples 1-3) and D+A samples (samples 7-14). For plot b) the AA-channel intensity data is used for for each of the three sites of the acceptor only (samples 4-6) and D+A samples (samples 7-14). For further details we refer to the text.*

Inserting the estimates for the parameters on the right-hand side ($\widehat{G} = 0.7$, $\widehat{G}_A = 5.5, \widehat{G}_D = 7.4$) as well as the values for the quantum yield of the Alexa-488 donor fluorophore ($q_D = 0.92$) and of the Alexa-555 acceptor fluorophore ($q_A = 0.10$) gives that $Q_D/Q_A \approx 0.1$. So, the quantum efficiency of the applied detector in the A-channel is approximately 10 times larger than in the D-channel.

8. Estimate of M_D. For randomly distributed donors and acceptors in the plane Wolber and Hudson (1979) provide an analytical expression for the sample mean FRET efficiency E as a function of: 1) the Förster distance R_0, 2) the acceptor concentration, and 3) the distance R of closest approach between a donor and an acceptor. Some of the limiting assumptions made in the derivation are: a) donors do not compete with each other for transfer to an acceptor, b) all donor-acceptor pairs have the same Förster distance and c) the area contributed by the donors and acceptors is negligible i.e. there are no excluded area effects. The general solution is stated as an integral expression which should be solved numerically, but Wolber and Hudson (1979) also provide the following convenient and accurate approximation:

$$E = 1 - (A_1 e^{-k_1 c_A} + A_2 e^{-k_2 c_A}), \tag{1}$$

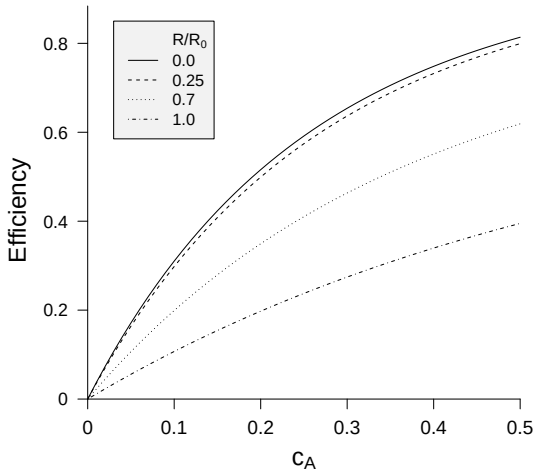

FIG 6. *Sample efficiency* (1) *for randomly distributed donors and acceptors in the plane as a function of* c_A*—i.e. the number of acceptors per area* R_0^2*—for various ratios of* R/R_0*, with* R_0 *the Förster distance of the donor-acceptor pair and* R *the distance of closest approach between a donor and an acceptor. Adapted from Wolber and Hudson (1979).*

with A_1, A_2, k_1, k_2 constants depending on the ratio of R/R_0 (see Table I in Wolber and Hudson, 1979) and c_A is the acceptor concentration in units of the number of acceptors per area R_0^2. In Figure 6 the efficiency as a function of the acceptor concentration is plotted for various R/R_0 ratios.

In the following we obtain an estimate for M_D by:

i) applying (1) to find an estimate of c_A—and thereby of the mean number of acceptor points within a pixel—for the samples prepared with the highest acceptor solution concentration of $[\mathrm{A}]_{\mathrm{sol}} = 8$,
ii) applying the equation for μ^i_{AA} in Section 2.2 of the main article, to find an estimate of M_D

Regarding i): The samples prepared with a solution concentration of $[\mathrm{A}]_{\mathrm{sol}} = 8$ are the samples 10, 12 and 14 (Table 1). The sample mean efficiencies of sample 10, 12 and 14, averaged over the three sites are 0.32, 0.45 and 0.59. We believe that due to the high concentrations of donors in sample 10 (applied donor solution concentration is 8), the donors in this sample compete with each other for energy transfer to surrounding acceptors, which leads to a much lower value of the efficiency than for samples 10 and 12. We therefore here exclude sample 10 from the analysis.[4].

[4]For a random distribution of donors and acceptors and under the assumption that donors do not compete for energy transfer to an acceptor the sample efficiency is inde-

The average sample mean efficiency of sample 12 and 14 for the three sites is 0.52. Assuming the value of closest approach R to be zero then by aid of Figure 6 we find that to $E = 0.55$ corresponds $c_A \approx 0.2$ [acceptors/R_0^2]. As for the Alexa-488 and Alexa-555 donor-acceptor pair $R_0 = 7$ nm, the average number of acceptors residing within a pixel of area 279×279 nm^2 for the samples 10 and 12 is approximately: $(0.2/(7^2)) \cdot 279^2 = 317.7 \approx 320$.

Regarding ii): Summing the equation for μ^i_{AA} in Section 2.2 of the main article on the left and right hand-side over all pixels $i = 1, \dots N$ on which our analysis is performed, i.e. the square subregion as displayed in Figure 1 to which will we refer here as W, results in

$$\sum_{i=1}^{N} \mu^i_{AA} = \frac{M_D}{K} \sum_{a \in \mathbf{x}_A \cap W} 1,$$

where $N = 1e4$. Rewriting yields

$$M_D = \frac{K}{n(\mathbf{x}_A \cap W)} \sum_{i=1}^{N} \mu^i_{AA}, \tag{2}$$

with $n(\mathbf{x}_A \cap W)$ denoting the total number of acceptor points in W. We find an estimate of M_D by finding estimates for $\sum_{i=1}^{N} \mu^i_{AA}$ and $n(\mathbf{x}_A \cap W)$ in (2) for the samples 12 and 14.

In Section 4 it was determined that the sample grand mean acceptor intensity $\bar{\bar{Y}}_{AA}$ scales with the sample acceptor concentration $[\mathrm{A}]_{\mathrm{sol}}$ by the slope $b_A = 15.4$. Thus for samples 12 and 14 we find that $\bar{\bar{Y}}_{AA} \approx 15.4 \cdot 8 = 123.2$.

Because the Bayesian inference method applied in the main article makes use of the aggregated data set summed over the ten measurements $m = 1, \dots, 10$, the sample mean of the aggregated AA-intensity for the samples 12 and 14 is—ignoring the photobleaching effect—approximately $10 \cdot 123.2 = 1232$, which provides an estimate of $\frac{1}{N} \sum_{i=1}^{N} \mu^i_{AA}$ for the aggregated data set. Further, the in this section found estimate for the the mean number of acceptors per pixel of 320 for the samples 12 and 14 is an estimate of $\frac{1}{N} n(\mathbf{x}_A \cap W)$. Applying the not rounded estimate of $\widehat{K} \approx 0.675$ previously found in Section 4, we find as an estimate for M_D, rounded to one decimal,

$$\widehat{M_D} \approx 0.675 \cdot \frac{1232}{320} = 2.6.$$

pendent of the donor concentration for a fixed acceptor concentration (Kenworthy and Edidin, 1998)

We note that the estimate of a mean number of 320 acceptors per pixel for the samples prepared with an acceptor solution concentration of 8 μg/ml is equally valid for donor fluorophores, i.e samples prepared with a donor solution concentration of $[\mathrm{D}]_{\mathrm{sol}} = 8\,\mu$g/ml will contain approximately 320 donors per pixel. Further, the two results can be extrapolated, i.e. the average numbers of acceptors and donors within a pixel are, respectively $40 \cdot [\mathrm{A}]_{\mathrm{sol}}$ and $40 \cdot [\mathrm{D}]_{\mathrm{sol}}$. We use the latter relations to specify the prior means of the Poisson point process intensities in Section 6.2 in the main article.

References.

Chen, H., Puhl, H. L., Koushik, S. V., Vogel, S. S. and Ikeda, S. R. (2006). Measurement of FRET efficiency and ratio of donor to acceptor concentration in living cells. *Biophysical journal* **91** L39–L41.

Clegg, R. M. (1996). Fluorescence Resonance Energy Transfer. In *Fluorescence Imaging Spectroscopy and Microscopy* (X. F. Wang and B. Herman, eds.) 179-252. Wiley and Sons, NY.

Elangovan, M., Wallrabe, H., Chen, Y., Day, R. N., Barroso, M. and Periasamy, A. (2003). Characterization of one-and two-photon excitation fluorescence resonance energy transfer microscopy. *Methods* **29** 58–73.

Johnson, I. (2010). *The Molecular Probes Handbook: A Guide to Fluorescent Probes and Labeling Technologies, 11th Edition*. Life Technologies Corporation.

Kenworthy, A. K. and Edidin, M. (1998). Distribution of a Glycosylphosphatidylinositol-anchored protein at the apical surface of MDCK cells examined at a resolution of¡ 100 AA using imaging fluorescence resonance energy transfer. *The Journal of cell biology* **142** 69–84.

Pawley, J. (2006). Fundamental limits in confocal microscopy. In *Handbook of biological confocal microscopy* (J. Pawley, ed.) 20-42. Springer.

Wallrabe, H., Chen, Y., Periasamy, A. and Barroso, M. (2006). Issues in confocal microscopy for quantitative FRET analysis. *Microscopy research and technique* **69** 196–206.

Wallrabe, H., Bonamy, G., Periasamy, A. and Barroso, M. (2007). Receptor complexes cotransported via polarized endocytic pathways form clusters with distinct organizations. *Molecular biology of the cell* **18** 2226–2243.

Wolber, P. K. and Hudson, B. S. (1979). An analytic solution to the Förster energy transfer problem in two dimensions. *Biophysical Journal* **28** 197–210.

Jan-Otto Hooghoudt
Aalborg University
Department of Civil Engineering
Aalborg, Denmark
E-mail: joh@civil.aau.dk

Margarida Barroso
Department of Molecular and Cellular Physiology
Albany Medical College
Albany, NY, USA
E-mail: barrosm@mail.amc.edu

Rasmus Waagepetersen
Aalborg University
Department of Mathematics
Aalborg, Denmark
E-mail: rw@math.aau.dk